INTERNATIONAL JOURNAL OF ADAPTIVE CONTROL AND SIGNAL PROCESSING
Int. J. Adapt. Control Signal Process. 2004; **18**:607–628
Published online in Wiley InterScience (www.interscience.wiley.com) DOI:10.1002/acs.823

An $\mathscr{H}_\infty$ algorithm for the windsurfer approach to adaptive robust control

Arvin Dehghani[1,2,*,†], Alexander Lanzon[1,2] and Brian D. O. Anderson[1,2]

[1] *Department of Systems Engineering, Research School of Information Sciences and Engineering, The Australian National University, Canberra, ACT 0200, Australia*
[2] *National ICT Australia Ltd., Locked Bag 8001, Canberra, ACT 2601, Australia*

SUMMARY

The windsurfing approach to iterative control requires a series of controller designs with the gradual expanding of the closed-loop bandwidth, and in the end in order to stop the algorithm, some validation tests are carried out. In this paper, an $\mathscr{H}_\infty$ design algorithm is introduced in order to remove the empirical aspect from the stopping criteria and to make the procedure more systematic, hence facilitating the design. Moreover, some restrictive assumptions on the plant model are lifted and some issues with the controller design step are tackled by the introduction of a new design method. This enables us to address a wider class of practical problems. Copyright © 2004 John Wiley & Sons, Ltd.

KEY WORDS: windsurfer approach; adaptive control; robust control; internal model control

1. INTRODUCTION

The iterative approach to designing a control system for a plant includes generally multiple steps, where a model of the true plant is used in a model-based control design method. The iteration includes improvement of the plant model, via re-identification, based on the information collected from the controlled plant, while operating under certain specified conditions, with a particular controller being connected, and redesigning of the controller based on the new model derived from re-identification.

As a result of extensive research on the understanding of the interplay between identification and control design, iterative redesign of controllers using data collected on the operating closed-loop system has emerged as a standard approach [1]. Some of the early examples of such iterative schemes are portrayed in References [2–4].

*Correspondence to: A. Dehghani, Department of Systems Engineering, The Australian National University, Canberra, ACT 0200, Australia.
† E-mail: arvin.dehghani@anu.edu.au

Contract/grant sponsor: ARC Discovery-Projects; contract/grant number: DP0342683
Contract/grant sponsor: National ICT Australia

 Accepted 22 June 2004

From one point of view, iterative control and re-identification is a form of adaptive control, e.g. papers such as Reference [2], and indeed this paper include the words 'adaptive control' in the title. A purist, however, might assert that there is distinction between adaptive control and iterative control and identification. In adaptive control, the identification and the controller design processes are almost always evolving at each instant of time or are almost always simultaneously in train. In iterative identification and control design, the processes of identification and controller design are kept separate in time. Identification occurs *between* two controller changes. In part, because of the intermingling of the identification and controller re-design objectives, the pure adaptive control scheme can result in some intrinsic problems; some are described in Reference [5].

The first is the transient instability problem, where there is a possibility that the controller connected to the plant, at a particular time, would yield an unstable closed-loop. Though the applied controller is not frozen in time, such controllers can frequently give rise to very large signal values in the closed-loop. A second problem is that of dealing with impractical control performance objectives; with the lack of full knowledge of the plant, the control objective may be impractical, but is not realized to be such in view of the lacking plant knowledge. A third problem is that of changing experimental conditions or controllers because a model of a plant which is a good model for one controller may be a bad model for another controller, and the adaptive control scheme uses a plant model rather than the plant itself as the basis for changing the controller.

Iterative control and identification addresses the first problem since virtually all algorithms seek to assure that any controller connected to the true plant after a redesign is stabilizing. Since that redesign is based on a model of the plant with a different controller, viz. that in use before the redesign, attention must be paid to the possibility inherent in the third difficulty mentioned above, viz. the inadequacy after change of controller of what was previously a good model. The inadequacy may be so great that the new controller destabilizes the true plant, though the performance prediction using the model may be excellent. Broadly, this difficulty is attacked by disallowing large controller changes [6–8]. We refer the reader to References [9–11] for details and for a survey on the iterative schemes.

One of the model-based iterative identification and control design methods, *the windsurfer approach*, was first introduced in Reference [12] with the aim of proposing an iterative algorithm which gradually broadens the bandwidth of a closed-loop system through repetition of a two-step procedure using identification and controller re-design steps. Hence, the algorithm, outlined e.g. in References [2, 13, 14], is constructed to achieve the desired performance and design objectives, in which the internal model control (IMC) method [15] is iteratively utilized in the controller design steps. In the case of *stable* plants, the IMC design method offers the advantage of simplicity and the fact that the closed-loop bandwidth of the system can be set via a single design parameter [2, 16]. However, if the plant is *unstable*, the same simple IMC design method cannot be used. Treatment of the unstable plant case can be found in papers [17, 18]. Nevertheless, there are some inadequacies with the IMC design methods for both stable and unstable plants which will be extensively discussed in Section 2.2.

In this paper, we introduce a modified algorithm for the windsurfer approach by incorporating a new controller design method. This new controller design method maintains the desirable features of the IMC design method, but also extends its applicability and addresses some of the IMC shortcomings, which are explicitly discussed in Section 2.2 and addressed in Section 2.3. The proposed algorithm introduces an $\mathscr{H}_\infty$ design technique in order to make the

windsurfer approach more systematic and to relax some restrictive assumptions on the plant. Furthermore, this $\mathscr{H}_\infty$ design technique deals with the potential IMC shortcomings directly at the controller design step.

Let us sketch an outline of this paper. In Section 2, we first review the IMC design method, noting the open issues. Then, we record the underlying assumptions for the proposed new algorithm. This includes the introduction of a new systematic controller design method that captures all the features of the IMC, but also addresses some inadequacies of the design method. Section 3 discusses the proposed windsurfer algorithm and we elaborate on the description of the algorithm. The algorithm is presented step-by-step in Section 3.1. In order to illustrate and give insight into the versatility of the proposed algorithm, an example is outlined in Section 4. To achieve this, we take a very detailed and step-by-step approach in presenting the example. We conclude this paper by emphasizing the highlights of the new algorithm and give some insights into further research in this area.

2. CONTROLLER DESIGN METHOD

2.1. An overview of IMC

IMC is a simple but effective control design method which has been successfully used in many applications where a desired closed-loop amplitude response from reference signal to plant output must be achieved. The effectiveness and simplicity of this method has led to many industrial applications (see Reference [19] and the references therein). This design method also guarantees a certain level of robust stability and robust performance in the sense described in Reference [15]. Furthermore, for a *stable* plant, adjustment of a single parameter directly and simply determines the closed-loop bandwidth and hence the reference tracking capabilities. Let us now outline the method for the stable plant case. The IMC structure is shown in Figure 1.

Consider a *SISO* stable model of the plant, P_i, with no zero on the jω-axis. Decompose P_i multiplicatively into a stable all-pass, $[P_i]_a$, and a stable minimum-phase, $[P_i]_m$, components, that is

$$P_i = [P_i]_a [P_i]_m \tag{1}$$

Let F_i be a low-pass filter, for example

$$F_i = \left(\frac{\lambda_i}{s+\lambda_i}\right)^n \tag{2}$$

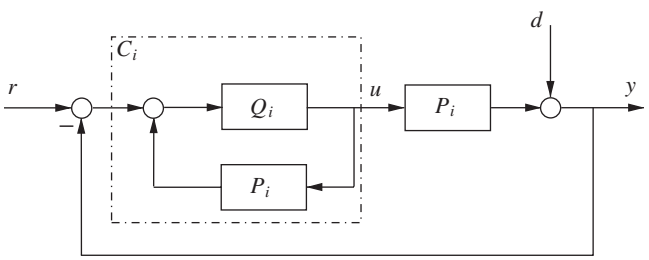

Figure 1. IMC structure.

specified by the designer and with amplitude response representing the amplitude response of the desired closed-loop transfer function. Then, the following controller (which has no unstable pole-zero cancellation with the plant):

$$C_i = \frac{Q_i}{1 - P_i Q_i} \tag{3}$$

with

$$Q_i = [P_i]_m^{-1} F_i \tag{4}$$

achieves a closed-loop bandwidth of λ_i and the desired closed-loop transfer function is given by

$$[T_i]_{yr} = \frac{P_i C_i}{1 + P_i C_i} = [P_i]_a F_i \tag{5}$$

Note that in the IMC design method, the positive integer n is chosen sufficiently large so that Q_i is proper.

Equation (5) reveals that the magnitude response of the designed closed-loop is exactly specified by the magnitude response of F_i. This implies that adjusting the filter time constant is equivalent to adjusting the speed of the closed-loop response.

Expressions (1)–(5) confirm the simple and efficient structure of the design method for stable plants. However, if the plant is *unstable*, the aforementioned filter bandwidth, λ_i, can no longer adjust the closed-loop bandwidth directly and the *simplicity* of the design method is replaced by a more *complex* procedure outlined in References [17, 18].

2.2. *Difficulties with the IMC approach*

Consider the feedback system in Figure 2. One can express y and u in terms of r_1 and r_2 as follows:

$$\begin{bmatrix} y \\ u \end{bmatrix} = \begin{bmatrix} \dfrac{P_i C_i}{1 + P_i C_i} & \dfrac{P_i}{1 + P_i C_i} \\ \dfrac{C_i}{1 + P_i C_i} & \dfrac{1}{1 + P_i C_i} \end{bmatrix} \begin{bmatrix} r_1 \\ r_2 \end{bmatrix} \tag{6}$$

where r_2 represents a second external input or disturbance acting on the plant input.

To motivate the importance of considering the four transfer functions in Equation (6), let us note some key points. The (1,1) transfer function $T_{yr_1} = P_i C_i/(1 + P_i C_i)$ is clearly important for reference tracking and the IMC design method deals specifically with this and only this. Special care, however, must be exercised in regard to the other three transfer functions as the IMC does not handle them explicitly. For a sensible design, the transfer function from plant input

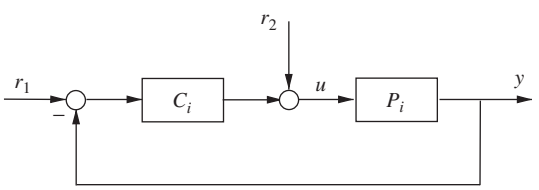

Figure 2. Standard feedback configuration.

disturbance to output, $T_{yr_2} = P_i/(1 + P_iC_i)$, must be maintained below a certain size since we wish plant input disturbances to be attenuated at the plant output. Likewise, $T_{ur_1} = C_i/(1 + P_iC_i)$ represents the transfer function from reference input to control signal and hence, must be kept below a certain size for a sensible design in order to avoid control actuator saturation and high-energy control action. Furthermore, the size of the four transfer functions in Equation (6) is related to a generalized robust stability margin [20] which corresponds to the amount of (coprime factor) uncertainty that can perturb P_i without destabilizing the loop [21]. The implication of these issues is discussed in more detail in the sequel.

With this introduction in mind, let us now record the circumstances where the above-described IMC design method cannot be properly used or is limited by restrictive assumptions.

(a) If P_i is unstable, then the simple IMC design method outlined in Section 2.1 cannot be used. If one seeks to use the method it fails because the internal stability of the loop in Figure 1 will be lost. There does exist a different IMC design method for the unstable plant case but the procedure is much more complicated (see References [17, 18]);
(b) If P_i has zeros on the jω-axis, then the decomposition in Equation (1) is not possible. If we relax the conditions on $[P_i]_m$ to allow it to contain these zeros, then Q_i in Equation (4) will not be stable and again internal stability of the loop in Figure 1 will be lost;
(c) If the model has lightly damped stable poles within the closed-loop passband, then $P_i/(1 + P_iC_i)$ will have large gain near the frequencies of those poles and hence any plant input disturbances at these frequencies are greatly magnified at the plant output;
(d) If the model has lightly damped stable/unstable zeros within the closed-loop passband, then $C_i/(1 + P_iC_i)$ will have large gain near the frequencies of those zeros, hence any reference signals at these frequencies result in very large control signal;
(e) If the bandwidth of F_i is much larger than the bandwidth of P_i, then $|C_i|$ will be very large at frequencies inside the bandwidth of F_i and outside the bandwidth of P_i, and again the control signal will be very large;
(f) If the roll-off rate of F_i is desired to be less than the roll-off rate of P_i (or equivalently $[P_i]_m$), then the outlined IMC design method will result in an improper controller, C_i, since Q_i becomes improper.

Notice that the IMC design method described in Section 2.1 fails and cannot be used in situations (a), (b), (f). On the contrary, the IMC design method can be applied in situations (c)–(e) but difficulties may occur.

The situations (c)–(e) imply that one of the transfer functions in the 4-block transfer function defined in Equation (6) will be large and the undesirable features described above will occur. For example, with situation (c), if a sinusoidal plant input disturbance signal with frequency close to the frequency of the plant lightly damped pole enters the loop at the input r_2, this disturbance will be greatly amplified by the large gain of T_{yr_2} near the frequency of the pole and will cause the output y to be severely affected. One can repeat this sort of argument for the other cases too. In the following subsection, we shall introduce a new controller design method that inherits the useful desired features of the IMC design method, but addresses problems (a)–(f) explicitly.

2.3. Proposed $\mathscr{H}_\infty$ controller design method

Principally, we would like to use the desired features of the IMC on either a stable or unstable plant, while ensuring that the magnitudes of all the transfer function matrix entries in

Equation (6) do not become too large. In other words, we wish to accomplish two objectives: to have $P_iC_i/(1+P_iC_i)$ close to $[P_i]_aF_i$ (even with P_i unstable or perhaps possessing a jω-axis zero), and to make sure that the other three transfer functions in Equation (6) do not assume large magnitudes.[‡]

These two objectives, however, are not the same and the need for reformulation of the problem in such a way to capture our objectives arises. Therefore, we shall introduce an $\mathscr{H}_\infty$ index and require this index to be minimized over all stabilizing controllers. We normally have performance objectives in mind, which requires some transfer functions to be small or below certain values in some frequency regions and other transfer functions small or below certain values at other frequencies. The $\mathscr{H}_\infty$ index will be weighted to achieve the desired effect. One should keep in mind that at the end of the day, it is a trade-off between keeping the size of $[P_iC_i/(1+P_iC_i)-[P_i]_aF_i]$ small and the size of the other three transfer functions in Equation (6) below certain values.

Let us outline our proposed controller design method.

(i) Given a model of the plant, P_i do the following factorization:

$$P_i=[P_i]_a[P_i]_m \quad \text{where} \begin{cases} [P_i]_a \in \mathscr{RH}_\infty, \quad [P_i]_a^{\sim}[P_i]_a=I \\ [P_i]_m \quad \text{has no zeros in } \mathbb{C}_+ \end{cases} \tag{7}$$

where $\mathbb{C}_+$ denotes the open right-half plane.

(ii) The admissible controller is given by solving the following $\mathscr{H}_\infty$ problem:

$$\gamma_i=\min_{C_i\in\underline{\mathscr{C}}}\left\|\begin{matrix} \dfrac{P_iC_i}{1+P_iC_i}-[P_i]_aF_i & \varepsilon_2(s)\dfrac{P_i}{1+P_iC_i} \\ \varepsilon_1(s)\dfrac{C_i}{1+P_iC_i} & \varepsilon_1(s)\varepsilon_2(s)\dfrac{1}{1+P_iC_i} \end{matrix}\right\|_\infty \tag{8}$$

where $\underline{\mathscr{C}}$ denotes the set of all proper stabilizing controllers for the plant, P_i, and $\varepsilon_1(s)$ and $\varepsilon_2(s)$ are SISO, stable, minimum-phase and proper weights.[§] We shall explain in detail the selection of the weighting functions in the following subsection.

One should note that all cases, (a)–(f), related to the difficulties with the IMC design method outlined in Section 2.2, are addressed by the proposed design method (e.g. this design method is applicable to stable or unstable plants, plants with or without jω-axis zeros, and the filter $F_i(j\omega)$ can have a roll-off rate larger or smaller than that of $P_i(j\omega)$, and so forth). This will become clear in the next section where we explain how $\varepsilon_1(s)$ and $\varepsilon_2(s)$ are chosen. For the moment, note that the (1,1) term in Equation (8) is making $P_iC_i/(1+P_iC_i)$ close to $[P_i]_aF_i$ (similarly to traditional IMC), the (1,2) term is limiting the size of $P_i/(1+P_iC_i)$, and the (2,1) term is limiting the size of $C_i/(1+P_iC_i)$. Furthermore, the set $\underline{\mathscr{C}}$ contains stabilizing proper

[‡]Note that the (2,2) transfer function, $1/(1+P_iC_i)$, in Equation (6) is directly related to the (1,1) transfer function, $P_iC_i/(1+P_iC_i)$, in a SISO setting and good design of $P_iC_i/(1+P_iC_i)$ implies good design of $1/(1+P_iC_i)$. In the MIMO case (which is not considered in this paper), however, $(I+C_iP_i)^{-1}$ is not so directly related to $P_i(I+C_iP_i)^{-1}C_i$ and hence the size of $(I+C_iP_i)^{-1}$ has to be directly controlled.

[§]Note that $\min_{C_i\in\underline{\mathscr{C}}}\|\mathscr{F}_l(.,.)\|_\infty$ rather than $\inf_{C_i\in\underline{\mathscr{C}}}\|\mathscr{F}_l(.,.)\|_\infty$ is used since we need both γ_i and $C_i\in\underline{\mathscr{C}}$. That is, the controller C_i must be proper and stabilizing and must achieve γ_i. In the cases we considered, the minimum is attained.

controllers and hence internal stability will always be achieved and the controller achieving this will always be proper.

The index in (8) can be rewritten as

$$\gamma_i = \min_{C_i \in \underline{\mathscr{C}}} \left\| \begin{bmatrix} 1 & 0 \\ 0 & \varepsilon_1(s) \end{bmatrix} \begin{bmatrix} \dfrac{P_i C_i}{1+P_i C_i} - [P_i]_a F_i & \dfrac{P_i}{1+P_i C_i} \\ \dfrac{C_i}{1+P_i C_i} & \dfrac{1}{1+P_i C_i} \end{bmatrix} \begin{bmatrix} 1 & 0 \\ 0 & \varepsilon_2(s) \end{bmatrix} \right\|_\infty \tag{9}$$

or alternatively

$$\gamma_i = \min_{C_i \in \underline{\mathscr{C}}} \left\| \mathscr{F}_l \left(\left[\begin{array}{cc|c} -[P_i]_a F_i & \varepsilon_2(s) P_i & P_i \\ 0 & \varepsilon_1(s)\varepsilon_2(s) & \varepsilon_1(s) \\ \hline 1 & -\varepsilon_2(s) P_i & -P_i \end{array} \right], \; C_i \right) \right\|_\infty \tag{10}$$

where the term in the square bracket is usually referred to as the generalized plant and $\mathscr{F}_l(.,.)$ denotes the lower linear fractional transformation.

One can easily verify that the assumptions of a standard $\mathscr{H}_\infty$ control problem for the generalized plant in Equation (10) are fulfilled when $\varepsilon_1(s)$ is chosen to be bi-proper. The reader is referred to References [21–23] for details on the $\mathscr{H}_\infty$ control problem and related discussions.

2.4. *Design of weighting functions* $\varepsilon_1(s)$ *and* $\varepsilon_2(s)$

We shall now discuss the design of the weighting functions that were introduced as a part of the $\mathscr{H}_\infty$ index in Equation (8). One should realize that based upon the particular application specifications and also the characteristics of the plant, we will have different objectives in different frequency regions. Let us now set out our design objectives, as specified in the index in Equation (8):

(1) Let α be the desired closeness between $P_i C_i/(1+P_i C_i)$ and $[P_i]_a F_i$ in an $\mathscr{H}_\infty$ sense. That is, we require $\|P_i C_i/(1+P_i C_i) - [P_i]_a F_i\|_\infty \leqslant \alpha$.
(2) Let β_p be the maximum tolerable gain in the appropriate frequency region for the transfer function $T_{yr_2} = P_i/(1+P_i C_i)$. That is, we require $\bar{\sigma}[P_i/(1+P_i C_i)(\mathrm{j}\omega)] \leqslant \beta_p, \;\; \forall \omega \in [\omega_1, \omega_2]$, where $\bar{\sigma}$ denotes the maximum singular value.
(3) Let β_c be the maximum tolerable gain in the appropriate frequency region for the transfer function $T_{ur_1} = C_i/(1+P_i C_i)$. That is, we require $\bar{\sigma}[C_i/(1+P_i C_i)(\mathrm{j}\omega)] \leqslant \beta_c, \;\; \forall \omega \in [\omega_3, \omega_4]$.

Now, we have three different numbers, i.e. α, β_p and β_c, that capture our objectives. These three numbers will be used to specify $\varepsilon_1(s)$ and $\varepsilon_2(s)$ as we discuss next. Once $\varepsilon_1(s)$ and $\varepsilon_2(s)$ are specified, we just need to check the number γ_i to determine whether the design was successful in achieving our objectives or not. Towards this end, note that the index in (8) certainly guarantees that

$$\bar{\sigma}\left[\frac{P_i C_i}{1+P_i C_i} - [P_i]_a F_i\right] \leqslant \gamma_i \quad \forall \omega \tag{11}$$

$$\bar{\sigma}\left[\frac{P_i}{1+P_iC_i}(j\omega)\right] \leqslant \frac{\gamma_i}{|\varepsilon_2(j\omega)|} \quad \forall\omega \tag{12}$$

$$\bar{\sigma}\left[\frac{C_i}{1+P_iC_i}(j\omega)\right] \leqslant \frac{\gamma_i}{|\varepsilon_1(j\omega)|} \quad \forall\omega \tag{13}$$

are achieved. Consequently, choosing $|\varepsilon_1(j\omega)| \geqslant \alpha/\beta_c \ \forall\omega \in [\omega_3, \omega_4]$ and $|\varepsilon_2(j\omega)| \geqslant \alpha/\beta_p \ \forall\omega \in [\omega_1, \omega_2]$ will do the trick since $\gamma_i \leqslant \alpha$ will mean that our three objectives in Equations (11)–(13) are satisfied.

Let us consider four different scenarios that describe how $\varepsilon_1(j\omega)$ and $\varepsilon_2(j\omega)$ ought to be chosen.

2.4.1. If $\varepsilon_1(j\omega) = 0$ *and* $\varepsilon_2(j\omega) = 0$. Then the $\mathscr{H}_\infty$ index specified in Equation (8) reduces to

$$\gamma_i = \min_{C_i \in \underline{\mathscr{C}}} \left\| \frac{P_iC_i}{1+P_iC_i} - [P_i]_a F_i \right\|_\infty \tag{14}$$

and hence C_i will be exactly the IMC controller[¶] described in Section 2.1, if P_i is stable and has no $j\omega$-axis zeros and all other assumptions of the IMC design method outlined in Section 2.1 are fulfilled (i.e. $\gamma_i = 0$ for such a case).[‖] Thus, $\varepsilon_1(j\omega)$ and $\varepsilon_2(j\omega)$ can be set to be very small in the frequency regions where the plant characteristics and our performance objectives are such that an IMC controller can perform well at those frequencies.

2.4.2. If $\varepsilon_1(j\omega) = 0$ *but* $\varepsilon_2(j\omega) \neq 0$. Then the $\mathscr{H}_\infty$ index specified in Equation (8) reduces to

$$\gamma_i = \min_{C_i \in \underline{\mathscr{C}}} \left\| \frac{P_iC_i}{1+P_iC_i} - [P_i]_a F_i \quad \varepsilon_2(s)\frac{P_i}{1+P_iC_i} \right\|_\infty \tag{15}$$

It is clear that, in this situation, we are trying to make $P_iC_i/(1+P_iC_i)$ close to $[P_i]_aF_i$ but simultaneously we are seeking to limit the size of $P_i/(1+P_iC_i)$. It was earlier discussed, (see Section 2.2), that if P_i had for example lightly damped poles in the closed-loop bandwidth, then an IMC controller would result in a transfer function, $P_i/(1+P_iC_i)$, that has large gain near the frequency of the lightly damped poles. It was also explained that this is highly undesirable in a sensible design.

Consequently, we choose $|\varepsilon_2(j\omega)| \geqslant \alpha/\beta_p$ near the frequencies of the lightly damped poles of P_i, as this will then limit the size of $P_i/(1+P_iC_i)$. Hence $\gamma_i \leqslant \alpha$ will imply $\bar{\sigma}[P_i/(1+P_iC_i)(j\omega) - [P_i]_aF_i(j\omega)] \leqslant \alpha \ \forall\omega$ and $\bar{\sigma}[P_i/(1+P_iC_i)(j\omega)] \leqslant \beta_p$ for all frequencies near the frequency of the lightly damped poles of P_i. Therefore, the closeness of $P_iC_i/(1+P_iC_i)$ to $[P_i]_aF_i$ is traded-off with limiting the size of $P_i/(1+P_iC_i)$ at the problematic frequencies.

2.4.3. If $\varepsilon_1(j\omega) \neq 0$ *but* $\varepsilon_2(j\omega) = 0$. Then the $\mathscr{H}_\infty$ index specified in Equation (8) reduces to

$$\gamma_i = \min_{C_i \in \underline{\mathscr{C}}} \left\| \begin{array}{c} \dfrac{P_iC_i}{1+P_iC_i} - [P_i]_a F_i \\ \varepsilon_1(s)\dfrac{C_i}{1+P_iC_i} \end{array} \right\|_\infty \tag{16}$$

[¶] Note though that the $\mathscr{H}_\infty$ index can be used even if the plant, P_i, is unstable or has $j\omega$-axis zeros, although γ_i may not be equal to zero in this case.

[‖] The minimum may not be attainable when P_i is unstable or has $j\omega$-axis zeros or the roll-off rate of F is smaller than that of P_i in which case there would be an infimum but not a minimum.

It is clear that, in this situation, we are trying to make $P_iC_i/(1+P_iC_i)$ close to $[P_i]_aF_i$ but limit the size of $C_i/(1+P_iC_i)$. It was earlier noted, (see Section 2.2), that if P_i had for example lightly damped zeros in the passband, then an IMC controller would result in a transfer function, $C_i/(1+P_iC_i)$, that has large gain near the frequency of the lightly damped zeros. It was also explained that this is highly undesirable in a sensible design.

Consequently, we choose $|\varepsilon_1(j\omega)| \geqslant \alpha/\beta_c$ near the frequencies of the lightly damped zeros of P_i, as this will limit the size of $C_i/(1+P_iC_i)$. Hence $\gamma_i \leqslant \alpha$ will imply $\bar{\sigma}[P_i/(1+P_iC_i)(j\omega) - [P_i]_aF_i(j\omega)] \leqslant \alpha\ \forall\omega$ and $\bar{\sigma}[C_i/(1+P_iC_i)(j\omega)] \leqslant \beta_c$ for all frequencies near the frequency of the lightly damped zeros of P_i. Therefore, the closeness of $P_iC_i/(1+P_iC_i)$ to $[P_i]_aF_i$ is traded-off with limiting the size of $C_i/(1+P_iC_i)$ at the problematic frequencies.

2.4.4. If $\varepsilon_1(j\omega) \neq 0$ *and* $\varepsilon_2(j\omega) \neq 0$. Then we can trade-off the closeness requirement of $P_iC_i/(1+P_iC_i)$ to $[P_i]_aF_i$ with limiting the size of both $P_i/(1+P_iC_i)$ and $C_i/(1+P_iC_i)$ at the appropriate frequencies. Again, $\varepsilon_1(j\omega)$ and $\varepsilon_2(j\omega)$ are chosen such that $|\varepsilon_1(j\omega)| \geqslant \alpha/\beta_c$ and $|\varepsilon_2(j\omega)| \geqslant \alpha/\beta_p$ at the appropriate frequencies.

3. NEW WINDSURFER APPROACH DESIGN PROCEDURE

The iterative control and identification approach to adaptive control includes two types of steps: identification and controller design steps. With a stabilizing controller acting on the true plant, a model of the plant is identified through a closed-loop identification procedure. One should realize that we now have two different systems; the closed-loop of the true plant and the controller, and the closed-loop of the identified model and the controller.

Then, a new controller is designed using the model with some closed-loop performance objectives through some design method. This controller design method should slowly and safely increase the closed-loop performance objectives until (as revealed by experimentation) there is a significant discrepancy between the closed-loop of the true plant and the last designed controller, and the closed-loop of the model and the last designed controller. Controller redesign ceases while a new model is identified, and the above-procedure is then repeated until the desired performance is achieved or no further improvement is possible.

As mentioned in the introduction, the originally proposed windsurfer approach to iterative identification and control re-design [2] gradually and safely increases the closed-loop bandwidth. Furthermore, it uses the IMC design method at the control stage. As extensively discussed in Section 2.2, the IMC design method suffers from some serious deficiencies. These are, however, all addressed in our new $\mathscr{H}_\infty$ design method (see Section 2.3).

Hence, in the sequel, we shall propose a *modified* windsurfer algorithm that makes use of our new $\mathscr{H}_\infty$ design method, instead of the IMC, at the control design step. Due to this change at the controller design step, we also modify other parts of the windsurfer algorithm to make it more amenable to our design method. It is important to understand that our new $\mathscr{H}_\infty$ design method is far better suited to flag when the re-identification is required, when compared to the IMC design method.

3.1. A modified iterative identification and controller re-design algorithm

Given a true physical plant, P_t, which is unknown, and a known controller, C_0, which stabilizes P_t, the algorithm follows the steps outlined below. We elaborate on the steps in the following section.

- *Step 1*: Perform the closed-loop identification so that the identified plant model P_i satisfies: $[P_i, C_i]$ stable and $\max_{1\leqslant k\leqslant N} \bar{\sigma}[H(P_t, C_i) - H(P_i, C_i)(j\omega_k)]$ small;**
- *Step 2*: Set an initial bandwidth, λ_0, for the desired closed-loop response, $F_i(j\omega)$. The initial bandwidth can be chosen to be much smaller than that of the identified model where its magnitude response is flat;
- *Step 3*: Find the critical frequency regions in P_i based on the cases, (a)–(f), discussed in Section 2.2. That is, find the frequency regions where P_i has lightly damped poles, lightly damped zeros or frequencies above the bandwidth of P_i but below the bandwidth of F_i.
  Based on the desired closed-loop objectives and specifications, set

(a) the positive number α to reflect the required closeness between $P_iC_i/(1 + P_iC_i)$ and $[P_i]_aF_i$, in the sense that $\|P_iC_i/(1 + P_iC_i) - [P_i]_aF_i\|_\infty \leqslant \alpha$.
(b) the positive numbers β_p and β_c to reflect the required maximum tolerable gain for $P_i/(1 + P_iC_i)$ and $C_i/(1 + P_iC_i)$, respectively, in the corresponding problematic frequency regions. That is

$$\bar{\sigma}\left[\frac{P_i}{1 + P_iC_i}(j\omega)\right] \leqslant \beta_p, \quad \forall\omega \in [\omega_1, \omega_2]$$

$$\bar{\sigma}\left[\frac{C_i}{1 + P_iC_i}(j\omega)\right] \leqslant \beta_c, \quad \forall\omega \in [\omega_3, \omega_4]$$

- *Step 4*: Design the frequency weights, $\varepsilon_1(s)$ and $\varepsilon_2(s)$, according to the rules given in Section 2.4, using the specified values α, β_p and β_c in Step 3, for the appropriate frequency regions;
- *Step 5*: Solve the $\mathscr{H}_\infty$ controller design problem given in Equation (8) and obtain γ_i and C_i;
- *Step 6*: If $\gamma_i \leqslant \alpha$ and $\max_{1\leqslant k\leqslant N} \bar{\sigma}[H(P_t, C_i) - H(P_i, C_i)(j\omega_k)]$ is small, then increase the bandwidth for F_i by 10%; and go to Step 5. Otherwise, go to Step 7;
- *Step 7*: Discard the last controller. IF there was a previous controller, then go to Step 1, else END.

In the first step of the algorithm, the identification procedure provides us with a model of the actual plant, P_0. Any closed-loop identification algorithm can be used although frequency domain identification methods are better suited to satisfy the frequency domain condition that $\max_{1\leqslant k\leqslant N} \bar{\sigma}[H(P_t, C_i) - H(P_i, C_i)(j\omega_k)]$ be small. The method we use is the one which is outlined in Reference [14] and the references therein.

The first step of the proposed $\mathscr{H}_\infty$ algorithm ensures an acceptable quality for the identified model and hence may result in a model which has higher order than the true plant.

**We use the notation $H(P_i, C_i)$ to refer to the 4-block transfer function defined in Equation (6).

We shall, however, emphasize that the purpose of our paper is not an exercise in identification. The identified model is utilized as a tool for the windsurfer algorithm and hence whether the model is of higher or lower order than the true plant is not important. Nevertheless, we perform model reduction based on the technique discussed in Reference [24] to avoid degree explosion.

The above-outlined algorithm has two different stopping criteria. One ensures that the closed-loop performance objectives set out in Step 3 of the algorithm are achieved ($\gamma_i \leqslant \alpha$). Once the desired closed-loop objectives are set in Step 3 by specifying three different numbers, i.e. α, β_p and β_c, we just need to check the number γ_i to determine whether the controller design was successful in achieving our objectives. The other stopping condition, $\max_{1 \leqslant k \leqslant N} \bar{\sigma}[H(P_t, C_i) - H(P_i, C_i)(j\omega_k)]$, takes care of the quality of obtained controller and guarantees acceptable performance of the controller in the closed-loop. Hence, the specific reasons for the discontinuation of the loop are manifested in Step 6.

In the following subsections, we discuss the underlying principles for the validation of the identified model, Step 1, and for choosing an initial bandwidth for the proposed new algorithm.

3.2. *Validation of the identified model*

Once a model of the true plant is identified, we need to validate the identified model by some criteria. We obviously require that the identified model is also stabilized by the same controller that is working on and stabilizing the true plant; this is a normal (though not universal) property of any closed-loop identification method. Also, to ensure frequency domain proximity, we require that the closed-loop transfer function describing the pair of the identified model and the controller, $[P_i, C_i]$, and the closed-loop transfer function describing the pair of the true plant and the controller, $[P_t, C_i]$, are close in a frequency by frequency sense (i.e. $\max_{1 \leqslant k \leqslant N} \bar{\sigma}[H(P_t, C_i) - H(P_i, C_i)(j\omega_k)]$ is small).

One should realize that P_i being close to P_t in an open-loop sense is not necessarily important. It is, however, of great significance to compare the two closed-loop transfer functions for frequencies excited by the controller. We, therefore, ensure that the closed-loop behaviours of the two pairs are close enough to each other through a closed-loop measure, viz. $\max_{1 \leqslant k \leqslant N} \bar{\sigma}[H(P_t, C_i) - H(P_i, C_i)(j\omega_k)]$.

We shall describe here the way to evaluate the term $\max_{1 \leqslant k \leqslant N} \bar{\sigma}[H(P_t, C_i) - H(P_i, C_i)(j\omega_k)]$ or an estimate of it in practice. We have P_i and C_i available in mathematical descriptions and therefore, can easily construct $H(P_i, C_i)$. But, $H(P_t, C_i)$ is not available in mathematical description due to the fact that P_t is an unknown physical entity. Consider the feedback structure in Figure 2 and Equation (6), the following lemma holds.

Lemma 3.1

For any P_t, P_i, C_i such that $[P_t, C_i]$ and $[P_i, C_i]$ are stable; that is a controller, C_i, which stabilizes both P_t and P_i; then for SISO systems

$$\bar{\sigma}[H(P_t, C_i) - H(P_i, C_i)] = \left[|C_i| + \frac{1}{|C_i|}\right] \left| \frac{P_t C_i}{1 + P_t C_i} - \frac{P_i C_i}{1 + P_i C_i} \right| \tag{17}$$

Proof

$$
\begin{aligned}
\bar{\sigma}[H(P_t, C_i) - H(P_i, C_i)] &= \bar{\sigma}\left[\begin{pmatrix} P_t \\ 1 \end{pmatrix} \frac{1}{1 + P_t C_i} (C_i \quad 1) - \begin{pmatrix} P_i \\ 1 \end{pmatrix} \frac{1}{1 + P_i C_i} (C_i \quad 1)\right] \\
&= \bar{\sigma}\left[\begin{pmatrix} \frac{P_t}{1+P_t C_i} - \frac{P_i}{1+P_i C_i} \\ \frac{1}{1+P_t C_i} - \frac{1}{1+P_i C_i} \end{pmatrix} (C_i \quad 1)\right] \\
&= \bar{\sigma}\left[\begin{pmatrix} \frac{P_t}{1+P_t C_i} - \frac{P_i}{1+P_i C_i} \\ -\frac{P_t C_i}{1+P_t C_i} + \frac{P_i C_i}{1+P_i C_i} \end{pmatrix} (C_i \quad 1)\right] \\
&= \bar{\sigma}\left[\begin{pmatrix} \frac{1}{C_i} \\ -1 \end{pmatrix} \left[\frac{P_t C_i}{1 + P_t C_i} - \frac{P_i C_i}{1 + P_i C_i}\right] (C_i \quad 1)\right] \\
&= \bar{\sigma}\left[\sqrt{\frac{1}{|C_i|^2} + 1} \left[\frac{P_t C_i}{1 + P_t C_i} - \frac{P_i C_i}{1 + P_i C_i}\right] \sqrt{|C_i|^2 + 1}\right] \\
&= \bar{\sigma}\left[\frac{\sqrt{|C_i|^2 + 1}}{|C_i|} \left[\frac{P_t C_i}{1 + P_t C_i} - \frac{P_i C_i}{1 + P_i C_i}\right] \sqrt{|C_i|^2 + 1}\right] \\
&= \bar{\sigma}\left[\left(\frac{|C_i|^2 + 1}{|C_i|}\right) \left[\frac{P_t C_i}{1 + P_t C_i} - \frac{P_i C_i}{1 + P_i C_i}\right]\right] \\
&= \left[|C_i| + \frac{1}{|C_i|}\right] \left|\frac{P_t C_i}{1 + P_t C_i} - \frac{P_i C_i}{1 + P_i C_i}\right|
\end{aligned}
$$

□

Note that the transfer function $P_t C_i/(1 + P_t C_i)$ in Equation (17) can be estimated at each frequency (over a dense grid of frequency points, $\{\omega_1, \ldots, \omega_N\}$) directly from measurement of $r_1(t)$ and $y(t)$, and $P_i C_i/(1 + P_i C_i)$ and $|C_i|$ can be analytically constructed.

3.3. Choosing an initial bandwidth

The plant model magnitude response, $|P_i(j\omega)|$, can provide a good starting point for setting the initial bandwidth of $F_i(j\omega)$. Special care, however, should be exercised in the case where the identified model has a resonant structure, or in other words, has lightly damped poles or zeros. It is always safe to choose the initial bandwidth of $F_i(j\omega)$ to be an order of magnitude less than the lowest predominant feature of $P_i(j\omega)$. That is, suppose if there is a resonant pole at ω_0 inside the plant bandwidth, choose the initial bandwidth for $F_i(j\omega)$ to be $\omega_0/10$.

4. NUMERICAL EXAMPLE

In this section, we consider a plant which is examined in References [2, 14] in order to discuss the proposed algorithm and also to show its systematic easy-to-use features.

Table I. Poles and zeros of $P_t(s)$.

$z_1 = -13.162$	$p_1, p_2 = -0.0996 \pm j3.0017$
$z_2, z_3 = -10.646 \pm j12.27$	$p_3, p_4 = -0.3339 \pm j12.131$
$z_4, z_5 = 7.169 \pm j11.54$	$p_5, p_6 = -1.8450 \pm j31.481$

The true plant is a robot arm with the following transfer function (depicted in Figure 5(a)):

$$P_t(s) = 0.5196 \frac{\prod_{i=1}^{5}(s - z_i)}{\prod_{i=1}^{6}(s - p_i)}$$

where poles and zeros are given in Table I.

The true plant has pairs of lightly damped poles with a pair of *RHP* zeros which will have impacts on the closed-loop bandwidth. We shall apply the algorithm described in Section 3.1. Note that, the windsurfer approach does not have available to it the mathematical description of the true plant; we only use this information to verify the method.

We use the closed-loop identification procedure detailed in Reference [25] and outlined in Reference [14]. The procedure showed how to convert a closed-loop identification problem into an open-loop identification problem. To start, the identification procedure requires an initial model of the plant and a controller that stabilizes both the model and the true plant. The initial model P_0 and the controller C_0 are chosen to be

$$P_0 = \frac{0.1709(s + 13.31)}{s^2 + 0.1806s + 9.024}, \quad C_0 = \frac{0.5849(s^2 + 0.1806s + 9.024)}{s(s + 13.31)}$$

The initial model, shown in Figure 5(a) together with $P_t(s)$, was obtained from [26]. Note that the controller is a standard IMC controller (Section 2.1) to achieve a closed-loop bandwidth of 0.1 rad/s.

Step 1 in our algorithm requires us to identify a plant model. Using the identification procedure of Hansen [25], we identify a model $\tilde{P}_1$ using P_0 and C_0 and the identification data collected. The (reference) input is chosen to consist of four periods of a zero-mean square wave of amplitude 1. The plant output was corrupted by zero-mean white noise with standard deviation of 0.05. The numerical subspace-based state space model estimation N4SID (built in MATLAB function) is used to estimate the model.

Choosing the identified Youla–Kucera parameter R (discussed in Reference [14]) to be of order five, the resulting identified model, $\tilde{P}_1$, is of degree 11. The magnitude response of $H(\tilde{P}_1, C_0)$ is shown in Figure 3 and $\tilde{P}_1(s)$ is given by

$$\tilde{P}_1(s) = 0.51819 \frac{1.0 \times 10^2 \prod_{i=1}^{10}(s - z_i)}{1.0 \times 10^2 \prod_{i=1}^{11}(s - p_i)}$$

with poles and zeros listed in Table II and its magnitude and phase response shown in Figure 4.

For this identified plant model $\tilde{P}_1$, $\max_{1 \leqslant k \leqslant N} \bar{\sigma}[H(P_t, C_0) - H(\tilde{P}_1, C_0)(j\omega_k)] = 0.4683$. Although one may think that 0.4683 is not small enough, we point out that (a) $\max_{1 \leqslant k \leqslant N} \bar{\sigma}[H(P_t, C_i) - H(G_1, C_i)(j\omega_k)] = 0.8637$, for the identified model G_1 in Reference [26], so our scheme is no worse; (b) It is very difficult for identification schemes to pick out the resonant structures of an unknown true plant at which frequencies this identification error is

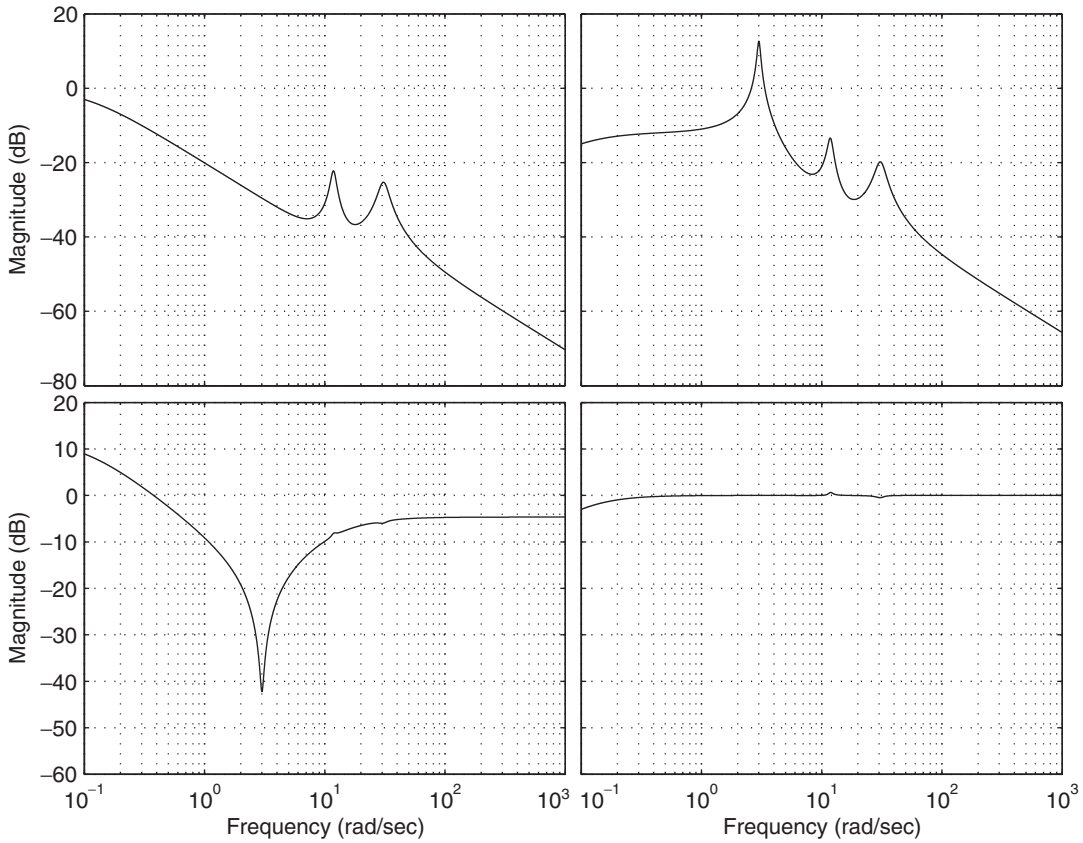

Figure 3. Magnitude responses of $H(\tilde{P}_1, C_0)$.

Table II. Poles and zeros of $\tilde{P}_1(s)$.

$z_1 = -0.0038$	$p_1 = -0.0039$
$z_2 = -0.1331$	$p_2 = -0.0041$
$z_3 = -8.9357$	$p_3 = -8.9357$
$z_4 = -0.0043$	$p_4, p_5 = -0.0297 \pm \text{j}0.3068$
$z_5, z_6 = 0.0628 \pm \text{j}0.1300$	$p_6, p_7 = -0.0070 \pm \text{j}0.1180$
$z_7, z_8 = -0.0658 \pm \text{j}0.0802$	$p_8, p_9 = -0.1130 \pm \text{j}0.0030$
$z_9, z_{10} = -0.1573 \pm \text{j}0.0109$	$p_{10}, p_{11} = -0.0009 \pm \text{j}0.0300$

occurring. In order to identify the unknown true plant more accurately, the input signal must have concentrated energy in the appropriate frequency regions. However, P_t is unknown and one cannot possibly identify the frequency regions which require particular excitation beforehand. Thus, one needs to use a generic input signal which has energy distributed over the whole range of frequency.

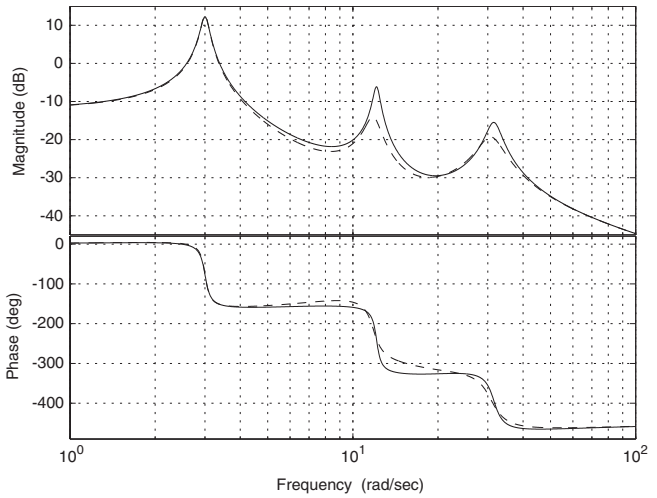

Figure 4. Magnitude and phase responses of P_t (*solid*) and $\tilde{P}_1$ (*dashed*).

Table III. Poles and zeros of $P_1(s)$.

$z_1 = -0.4052$	$p_1 = -0.4041$
$z_2, z_3 = 6.2812 \pm \text{j}13.0022$	$p_2 = -11.3789$
$z_4, z_5 = -16.7945 \pm \text{j}3.9365$	$p_3, p_4 = -2.9642 \pm \text{j}30.6857$
$z_6, z_7 = -6.5037 \pm \text{j}8.0120$	$p_5, p_6 = -0.6968 \pm \text{j}11.7983$
	$p_7, p_8 = -0.0903 \pm \text{j}3.0027$

One should realize that in the course of operating the iterative algorithm, each estimate of the plant is likely to be of higher degree than the previous one. In order to avoid degree explosion in the identified model, we employ the closed-loop model reduction method detailed in Section 4.3 of Reference [24, pp. 137–140]. Assume that the Hankel singular values of the graph symbols of the identified model are decreasingly ordered ($\sigma_1 > \sigma_2 > \sigma_3 > \cdots > \sigma_N$) and suppose $\sigma_r \ll \sigma_1$ for some r. The singular values for this case are $2.1976, 2.0657, 1.5216, 0.11324, 0.1191, 0.0801, 0.0552, 0.0460, 0.0002, 2.84\text{e}-5, 7.38\text{e}-10$. We perform balanced realization and the result is truncated to retain all Hankel singular values greater than $0.01\sigma_1$. The resulting model after truncation is

$$P_1(s) = 0.51893 \frac{\prod_{i=1}^{7}(s - z_i)}{\prod_{i=1}^{8}(s - p_i)}$$

with poles and zeros listed in Table III.

The identified plant P_1 is stabilized by C_0, ($[P_1, C_0]$ is stable), and we estimate $\max_{1 \leqslant k \leqslant N} \bar{\sigma}[H(P_t, C_0) - H(P_1, C_0)(\text{j}\omega_k)] = 0.4684$ (based on the procedure explained in Section 3.2). Hence the conditions in the first step of algorithm (outlined in Section 3.1) are met. The magnitude responses of the true plant $P_t(\text{j}\omega)$ and the model $P_1(\text{j}\omega)$ are shown in Figure 5(b).

The first peak in the magnitude response of the model P_1 happens close to 3 rad/s and hence the initial bandwidth, λ_1 is set to 0.1, which is much smaller than that of P_1 and is well below the first resonant frequency.

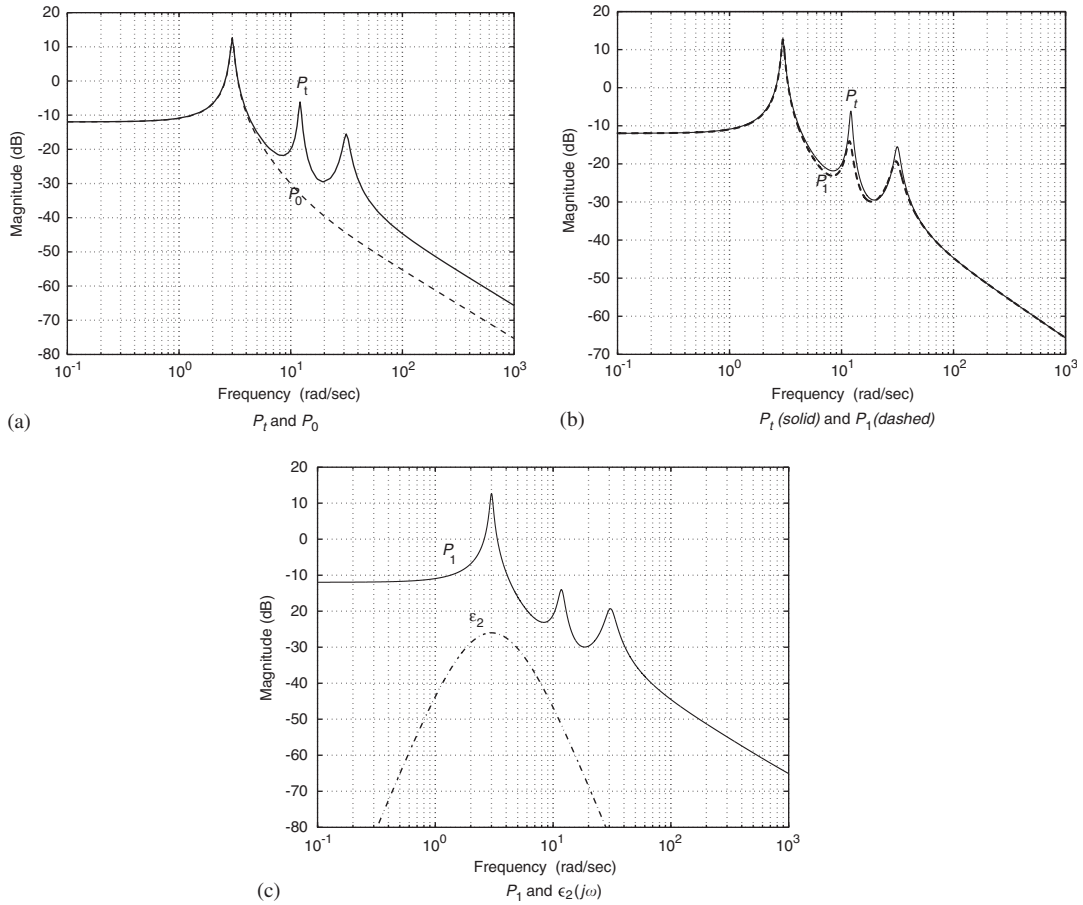

Figure 5. Magnitude responses: (a) P_t and P_0; (b) P_t (*solid*) and P_1 (*dashed*); and (c) P_1, and $\varepsilon_2(j\omega)$.

The model P_1 has three pairs of lightly damped poles and hence its magnitude response exhibits three peaks at the resonant frequencies. The right-half plane zeros will limit the closed-loop bandwidth that can be attained. Therefore, the critical frequency regions in P_1 are where it has lightly damped poles (p_3–p_8). As discussed in Section 2.4, we divide the plant model frequency response into two regions; *region 1*: below 1.5 rad/s, and *region 2*: contains the frequencies around the first resonant mode.

We shall now set our closed-loop performance objectives, as discussed in Step 3 of our algorithm and in Section 2.4, to: (i) have the closeness between $P_iC_i/(1 + P_iC_i)$ and $[P_i]_aF_i$ in an $\mathscr{H}_\infty$ sense below 0.1 ($\alpha = 0.1$); (ii) keep T_{yr_2} below $\beta_p = 2(\approx 6$ dB). Note that (ii) effectively limits the effect of the first resonant mode as we expand the bandwidth to frequencies that are close to 3 rad/s.

Based on the rules stated in Section 2.4 and the afore-stated desired closed-loop objectives, the frequency costs $\varepsilon_1(j\omega)$ and $\varepsilon_2(j\omega)$ are designed. Here, the closed-loop bandwidth λ_1 lies in the *first region*, hence $\varepsilon_1(j\omega)$ is set to be small (say 0.001), and $\varepsilon_2(j\omega)$ is chosen to take care of the first resonant mode of the plant model occurring at 3 rad/s. In the case of P_1, $\varepsilon_2(j\omega)$ is set to have the

maximum gain of -26 dB, ($\alpha/\beta_p = 0.1/2 = 0.05 \simeq -26$ dB). The frequency response of $\varepsilon_2(j\omega)$ and $P_1(j\omega)$ are shown in Figure 5(c).

As stated in Step 5 of our algorithm, we then solve the $\mathscr{H}_\infty$ index in Equation (10) with $F_1 = \lambda_1/(s+\lambda_1)$ and the controller obtained achieves the norm value of 0.10 ($\gamma_1 = 0.10 \leqslant \alpha$). The second condition in Step 6 of our algorithm, $\max_{1\leqslant k\leqslant N} \bar{\sigma}[H(P_t, C_i) - H(P_i, C_i)(j\omega_k)] = 0.3136$ and therefore both conditions in Step 6 of the algorithm are met. We increase the closed-loop bandwidth by 10% ($\lambda_2 = 0.11$) and go back to Step 5 as stated in the algorithm. The results as we loop between Steps 5 and 6 are given in Table IV. The two conditions of Step 6 are met until we push out the bandwidth to $\lambda_i = 1.0$ where $\gamma_i = 0.09 < \alpha$ but the difference in $\mathscr{H}_\infty$ sense between the closed-loop transfer function describing the pair $[P_1, C_i]$ and that of the pair $[P_t, C_i]$ has increased to a value greater than the initial one (0.4684) hence not anymore satisfactory ($\max_{1\leqslant k\leqslant N} \bar{\sigma}[H(P_t, C_i) - H(P_i, C_i)(j\omega_k)] = 0.4698$). This points out that re-identification is necessary. Therefore, we discard the last controller and go back to Step 1 for re-identification.

We again do the closed-loop identification as outlined above with P_1 and the controller that achieved the closed-loop bandwidth of $\lambda_i = 0.98$ rad/s and met the conditions of Step 6. To ensure that the input signal is sufficiently exciting (see proceeding discussion on energy concentration at the frequencies of the resonant modes), the input is chosen to consist of sinusoids with three different frequencies (3.0, 12.0, 31.0 rad/s) in the resonant frequency regions and of amplitude 0.1. This is superimposed on four periods of a zero-mean square wave of amplitude 1 which was our previously given generic signal. The plant output was corrupted by zero-mean white noise with standard deviation of 0.05.

Choosing the identified Youla–Kucera parameter R to be of order five, the resulting identified model is of degree 13 and $\tilde{P}_2(s)$ is given by

$$\tilde{P}_2(s) = 0.49884 \frac{\prod_{i=1}^{7} (s - z_i)}{\prod_{i=1}^{8} (s - p_i)}$$

with poles and zeros listed in Table V.

For this identified plant model $\tilde{P}_2$, $\max_{1\leqslant k\leqslant N} \bar{\sigma}[H(P_t, C_i) - H(\tilde{P}_2, C_i)(j\omega_k)] = 0.2619$.

Performing balanced realization and truncating this to retain all Hankel singular values greater than $0.01\sigma_1$, the resulting new identified model P_2 is

Table IV. Gradual expansion of closed-loop bandwidth.

λ_i	$\max_{1\leqslant k\leqslant N} \bar{\sigma}[H(P_t, C_i) - H(P_1, C_i)(j\omega_k)]$	γ_i
0.1	0.3265	0.10
0.11	0.3272	0.08
0.12	0.3281	0.08
0.13	0.3289	0.09
0.14	0.3297	0.1
0.16	0.3306	0.09
⋮	⋮	⋮
0.98	0.4661	0.1
1.0	0.4698	0.09

Table V. Poles and zeros of $\tilde{P}_2(s)$.

$z_1 = -13.3100$	$p_1 = -11.4917$
$z_2 = -12.6314$	$p_2 = -11.0354$
$z_3 = -6.9571$	$p_3 = -0.4889$
$z_4 = -0.6374$	$p_4 = -0.3186$
$z_5, z_6 = -11.7790 \pm \text{j}13.5731$	$p_5 = -0.2385$
$z_7, z_8 = 9.4603 \pm \text{j}10.5069$	$p_6, p_7 = -1.8397 \pm \text{j}31.5167$
$z_9, z_{10} = -0.3958 \pm \text{j}3.0249$	$p_8, p_9 = -0.3527 \pm \text{j}12.1210$
$z_{11}, z_{12} = -0.2538 \pm \text{j}0.0312$	$p_{10}, p_{11} = -0.0903 \pm \text{j}3.0027$
	$p_{12}, p_{13} = -0.3958 \pm \text{j}3.0249$

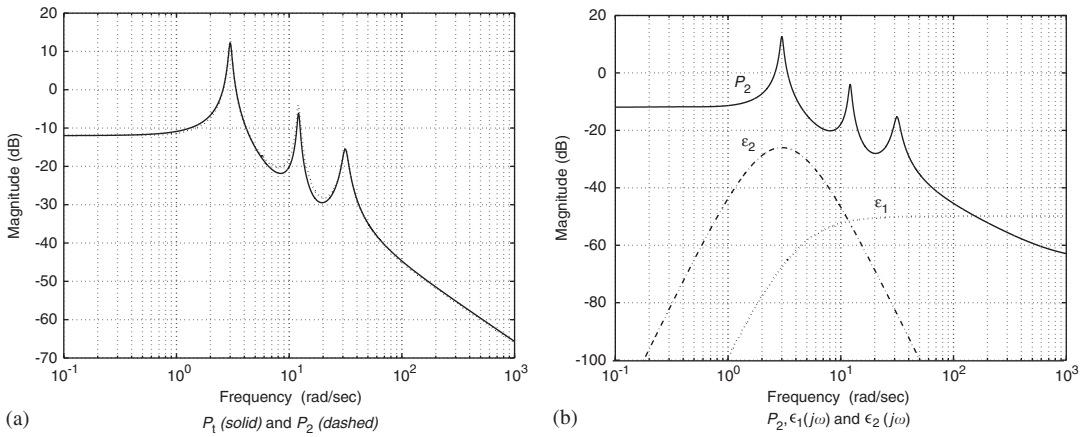

Figure 6. Magnitude responses: (a) P_t (*solid*) and P_2 (*dashed*); and (b) P_2, $\varepsilon_1(\text{j}\omega)$ and $\varepsilon_2(\text{j}\omega)$.

$$P_2(s) = 0.49831 \times \frac{(s+14.79)(s+7.037)(s+0.666)(s+0.318)(s^2-18.92s+200)(s^2+23.39s+321.3)}{(s+11.22)(s+0.521)(s+0.362)(s^2+0.18s+9.024)(s^2+0.70s+147)(s^2+3.68s+996.7)}$$

The identified plant P_2 is stabilized by C_i, ($[P_2, C_i]$ is stable), and we estimate $\max_{1\leqslant k\leqslant N} \bar{\sigma}[H(P_\text{t}, C_i) - H(P_2, C_i)\ (\text{j}\omega_k)] = 0.2620$, hence the conditions in the first step of our algorithm are met. The magnitude responses of the true plant $P_\text{t}(\text{j}\omega)$ and the model $P_2(\text{j}\omega)$ are shown in Figure 6(a).

The model P_2 has almost the same structure as P_1 with three pairs of lightly damped poles. The right-half plane zeros will limit the closed-loop bandwidth that can be attained. As discussed in Section 2.4, we now divide the plant model frequency response into three regions; *region 1*: below 1.5 rad/s, *region 2*: contains the frequencies around the resonant poles, and *region 3*: contains frequencies above the bandwidth of $P_2(\text{j}\omega)$ but below that of $F(\text{j}\omega)$, when λ_i becomes sufficiently large to exceed the bandwidth of $P_2(\text{j}\omega)$.

We shall now set our closed-loop performance objectives, as discussed in Section 2.4, to: (i) have the closeness between $P_iC_i/(1 + P_iC_i)$ and $[P_i]_aF_i$ in an $\mathscr{H}_\infty$ sense below 0.1 ($\alpha = 0.1$); (ii) keep T_{yr_2} below $\beta_p = 2$ (≈ 6 dB); and (iii) keep T_{ur_1} below $\beta_c = 30$ (≈ 30 dB). Note that the nature of β_p and β_c are different as the former refers to limiting the effects of the resonant

modes while the latter refers to the situation where we require higher closed-loop bandwidth than that of the plant. Here we assume that the actuators can pump up a maximum gain of 30, which is considered satisfactory for this robot arm example.

Based on the rules stated in Section 2.4 and the afore-stated desired closed-loop objectives, the frequency costs $\varepsilon_1(j\omega)$ and $\varepsilon_2(j\omega)$ are designed. The frequency cost $\varepsilon_1(j\omega)$ is chosen to gradually reach the maximum gain of almost -50 dB ($\alpha/\beta_c = \frac{0.1}{30}$) at 4 rad/s, where the plant model loses its bandwidth to the controller. The cost $\varepsilon_2(j\omega)$ is chosen to take care of the first resonant mode of the plant model occurring at 3 rad/s. In the case of P_2, $\varepsilon_2(j\omega)$ is set to have the maximum gain of -26 dB, ($\alpha/\beta_p = \frac{0.1}{2} = 0.05 \simeq -26$ dB). The frequency responses of $\varepsilon_1(j\omega)$, $\varepsilon_2(j\omega)$ and $P_2(j\omega)$ are shown in Figure 6(b).

If we gradually (10% in each iteration) increase the closed-loop bandwidth λ_i to 8.2 rad/s, γ_i increases to $0.134 > \alpha$ which indicates that the performance specifications are not satisfied and $\max_{1 \leqslant k \leqslant N} \bar{\sigma}[H(P_t, C_i) - H(P_2, C_i)(j\omega_k)] = 0.5678$ which indicates poor modelling.

When re-identification is performed, the closed-loop bandwidth can be further pushed out to 11.2 rad/s. After re-identification, the bandwidth cannot be increased more than 11.2 rad/s as γ_i will be more than 0.1 ($> \alpha$) and the performance objectives will hence not be met. The frequency response of P_t and $P_3(j\omega)$ are shown in Figure 7(a) and the frequency response of the final controller is depicted in Figure 7(b). The four transfer functions of $H(P_3, C_i)$ for $\lambda = 11.2$ rad/s are shown in Figure 7(c).

Let us now record a number of key attributes which make our proposed algorithm much more suitable for the windsurfer approach to iterative identification and control. The above example and the discussion in Section 2.3 and Steps 3–5 in the algorithm assert that our proposed $\mathscr{H}_\infty$ controller design method does offer simplicity and has an easy-to-use procedure. The parameters α, β_p and β_c capture our closed-loop objectives and specifications and are used to specify $\varepsilon_1(s)$ and $\varepsilon_2(s)$ as discussed in Section 2.4 and shown in the above example. They, however, are not *a priori* and/or complementary information about the plant.

The results in Reference [26] show that the closed-loop bandwidth can be expanded to 12 rad/s whereas ours can be expanded to 11.2 rad/s. Considering the 4-block transfer function $H(G_1, C_{\mathrm{IMC}})$, where G_1 denotes the identified model used in Reference [26] and C_{IMC} refers to the controller designed to achieve the close-loop bandwidth of 12 rad/s, we note the following important points:

- the magnitude response of the transfer function $G_1 C_{\mathrm{IMC}}/(1 + G_1 C_{\mathrm{IMC}})$ is exactly specified by the IMC filter $F = 12/(s+12)^2$ and hence exact reference tracking is achieved for the desired bandwidth on the identified model. However,

$$\max_{1 \leqslant k \leqslant N} \bar{\sigma}\left[\frac{P_t C_{\mathrm{IMC}}}{1 + P_t C_{\mathrm{IMC}}} - \frac{G_1 C_{\mathrm{IMC}}}{1 + G_1 C_{\mathrm{IMC}}}(j\omega_k)\right] = 0.57$$

  which indicates a large discrepancy in reference tracking capabilities if this controller, C_{IMC}, is chosen to be used on the true plant. On the contrary, our proposed algorithm ensures

$$\max_{1 \leqslant k \leqslant N} \bar{\sigma}\left[\frac{P_t C_i}{1 + P_t C_i} - \frac{P_i C_i}{1 + P_i C_i}(j\omega_k)\right] \approx 0.1$$

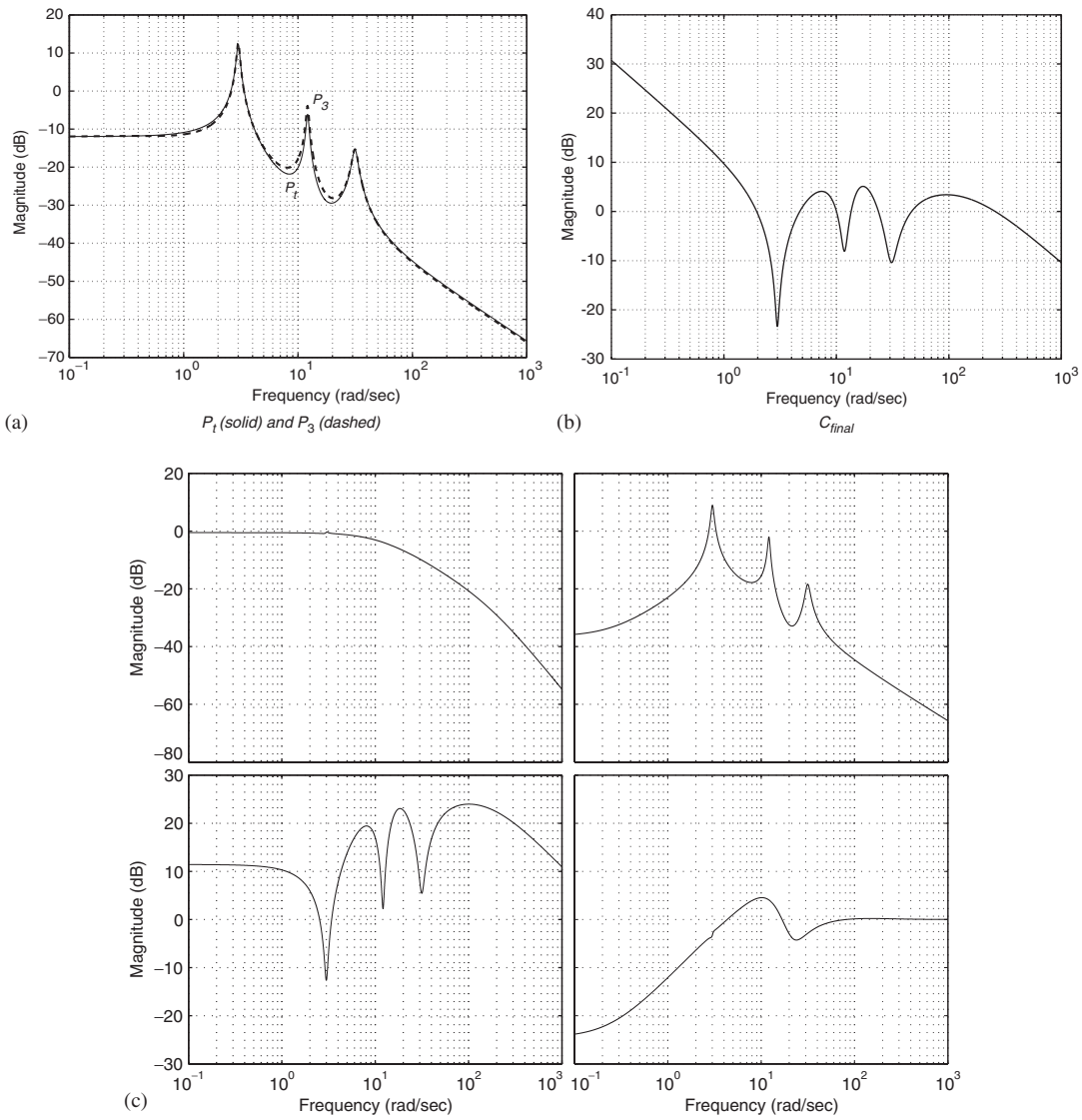

Figure 7. Magnitude responses: (a) P_{t} (*solid*) and P_3 (*dashed*); (b) C_{final}; and (c) $H(P_3, C_{\mathrm{final}})$.

for the maximum achievable bandwidth (i.e. 11.2 rad/s). This means that we have managed to expand the closed-loop bandwidth to approximately the same value as in [26] but kept

$$\max_{1 \leqslant k \leqslant N} \bar{\sigma}\left[\frac{P_{\mathrm{t}}C_i}{1 + P_{\mathrm{t}}C_i} - \frac{P_iC_i}{1 + P_iC_i}(\mathrm{j}\omega_k)\right]$$

small as required by our specifications.

- the transfer function $G_1/(1 + G_1C_{\mathrm{IMC}})$ has a maximum gain of approximately 10 dB since in the algorithm of Lee *et al.* [26] there was nothing limiting this gain but our method gives $\bar{\sigma}[P_i/(1 + P_iC_i)] \simeq 6.8$ dB;
- both $C_{\mathrm{IMC}}/(1 + G_1C_{\mathrm{IMC}})$ of Lee *et al.* [26] and our $C_i/(1 + P_iC_i)$ had a gain less than 30 dB and hence with respect to this criterion, both designs were satisfactory;
- for the design of Lee *et al.* [26], $\max_{1\leqslant k\leqslant N} \bar{\sigma}[H(P_{\mathrm{t}}, C_{\mathrm{IMC}}) - H(G_1, C_{\mathrm{IMC}})(\mathrm{j}\omega_k)] = 2.1530$ whereas in our algorithm $\max_{1\leqslant k\leqslant N} \bar{\sigma}[H(P_{\mathrm{t}}, C_{\mathrm{final}}) - H(P_3, C_{\mathrm{final}})(\mathrm{j}\omega_k)] = 0.257$. This shows that the final controller of Lee *et al.* [26] performs differently in a closed-loop sense on P_{t} than on G_1. The difference in closed-loop transfer functions of our final controller on P_{t} and on P_3 is well contained.
- The closed-loop bandwidth was increased to 3 rad/s in the design of Lee *et al.* [26] with the first model. The striking fact is that $\max_{1\leqslant k\leqslant N} \bar{\sigma}[H(P_{\mathrm{t}}, C_{\mathrm{IMC}}) - H(G_0, C_{\mathrm{IMC}})(\mathrm{j}\omega_k)] = 13.33$ where C_{IMC} denotes the IMC controller that achieved the closed-loop bandwidth of 3 rad/s and G_0 is the first model considered. This shows that the controller of Lee *et al.* [26] performs much differently in a closed-loop sense on P_{t} than on G_0. In contrast, our algorithm does not allow this discrepancy and is easily seen Table IV.

These points clearly show the superiority of our algorithm compared to the one of Lee *et al.* [26] in terms of keeping $P_{\mathrm{t}}C_i/(1 + P_{\mathrm{t}}C_i)$ close to $P_iC_i/(1 + P_iC_i)$, limiting the size of $P_i/(1 + P_iC_i)$, limiting the size of $C_i/(1 + P_{\mathrm{t}}C_i)$, and ensuring that the flags γ_i and $\max_{1\leqslant k\leqslant N} \bar{\sigma}[H(P_{\mathrm{t}}, C_i) - H(P_i, C_i)(\mathrm{j}\omega_k)]$ are easy to handle.

5. CONCLUSION

In this paper, we have introduced a modified algorithm for the windsurfer approach to iterative identification and control by incorporating a new controller design method. The proposed algorithm uses an $\mathscr{H}_\infty$ control design method, in which the shortcomings and deficiencies of the previously used IMC design methods [2, 17], are addressed. For instance, this $\mathscr{H}_\infty$ design method is applicable to stable or unstable plants or plants with jω-axis zeros. In addition, it handles plants well with lightly damped poles and zeros and situations where the bandwidth of F_i is orders of magnitude greater than that of P_i. This algorithm also gives us one number, γ_i, that easily flags whether the desired performance specifications have been achieved. Furthermore, an easy computation $\max_{1\leqslant k\leqslant N} \bar{\sigma}[H(P_{\mathrm{t}}, C_i) - H(P_i, C_i)(\mathrm{j}\omega_k)]$ indicates whether re-identification is necessary or not. In order to illustrate and give insight into the versatility of the proposed algorithm, a numerical example was discussed to show how systematic the bandwidth of the closed-loop system can be increased.

ACKNOWLEDGEMENTS

This work was supported by an ARC Discovery-Projects Grant (DP0342683) and National ICT Australia. National ICT Australia is funded through the Australian Government's *Backing Australia's Ability* initiative, in part through the Australian Research Council.

REFERENCES

1. Gevers M. A decade of progress in iterative control design: from theory to practice. In *Symposium on Advanced Control of Chemical Processes*, vol. 2, Pisa, Italy, 2000; 677–694.
2. Lee WS, Anderson BDO, Kosut RL, Mareels IMY. A new approach to adaptive robust control. *International Journal of Adaptive Control and Signal Processing* 1993; **7**(3):183–211.
3. Zang Z, Bitmead RR, Gevers M. Iterative model refinement and control robustness enhancement. In *Proceedings of the 30th IEEE Conference on Decision and Control*, Brighton, UK, 1991; 279–284.
4. Schrama RJP, Van den Hof PMJ. An iterative scheme for identification and control design based on coprime factorizations. In *Proceedings of the American Control Conference*, Chicago, IL, 1992; 2842–2846.
5. Anderson BDO, Gevers M. Fundamental problems in adaptive control. In *Perspectives in Control Theory and Applications*, Normand-Cyrot D (ed.). Springer: Berlin, 1998; 9–21.
6. De Callafon RA, Van den Hof PMJ. Suboptimal feedback control by a scheme of iterative identification and control design. *Mathematical Modelling of Systems* 1997; **3**(1):77–101.
7. Anderson BDO, Bombois X, Gevers M, Kulcsar C. Caution in iterative modelling and control design. In *IFAC Workshop on Adaptive Control and Signal Processing*, Glasgow, 1998; 13–19.
8. Gevers M, Bombois X, Codrons B, De Bruyne F, Scorletti G. The role of experimental conditions in model validation for control. In *Robustness in Identification and Control-Proceedings of Siena Workshop, July 1998*, Garulli A, Tesi A, Vicino A (eds). Springer: Berlin, 1999; **245**:72–86.
9. Bitmead RR. Iterative control design approaches. In *Proceedings of the 12th IFAC World Congress*, Sydney, vol. 9, 1993; 381–384.
10. Gevers M. Towards a joint design of identification and control? In *Essays on Control: Perspectives in the Theory and its Applications*, Trentelman HL, Willems JC (eds). Birkhauser, New York, 1993; 111–151.
11. Van den Hof PMJ, Schrama RJP. Identification and control: closed-loop issues. *Automatica* 1995; **31**:1751–1770.
12. Anderson BDO, Kosut RL. Adaptive robust control: on-line learning. In *Proceedings of the 30th IEEE Conference on Decision and Control*, Brighton, UK, 1991; 297–298.
13. Lee WS, Anderson BDO, Kosut RL, Mareels IMY. On robust performance improvement through the windsurfer approach to adaptive robust control. In *Proceedings of the 32nd IEEE Conference on Decision and Control*, San Antonio, TX, 1993; 2821–2827.
14. Anderson BDO. Windsurfing approach to iterative control design. In *Iterative Identification and Control*, Albertos P, Sala A (eds). Springer: Berlin, 2002; 143–166.
15. Morari M, Zafiriou E. *Robust Process Control*. Prentice-Hall: Englewood Cliffs, NJ, 1989.
16. Lee WS, Anderson BDO, Mareels IMY, Kosut RL. On some practical issues in system identification for the windsurfer approach to adaptive robust control. In *Proceedings of the 10th IFAC Symposium on System Identification*, 1994.
17. Lee WS, Mareels IMY, Anderson BDO. Iterative identification and two step control design for partially unknown unstable plants. *International Journal of Control* 2001; **74**(1):43–57.
18. Campi M, Lee WS, Anderson BDO. New filters for internal model control design. *International Journal of Robust and Nonlinear Control* 1994; **4**:757–775.
19. Garcia CE, Morari M. Internal Model Control. 1. A unifying review and some new results. *Industrial & Engineering Chemistry Process Design and Development* 1982; **21**:308–323.
20. Vinnicombe G. *Uncertainty and Feedback: $\mathscr{H}_\infty$ Loop Shaping and the v-gap Metric*. Imperial College Press: London, 2001.
21. Zhou K, Doyle JC, Glover K. *Robust and Optimal Control*. Prentice-Hall: Englewood Cliffs, NJ, 1995.
22. Zhou K, Doyle JC. *Essentials of Robust Control*. Prentice-Hall: Englewood Cliffs, NJ, 1998.
23. Green M, Limebeer DJN. *Linear Robust Control*. Prentice-Hall: Englewood Cliffs, NJ, 1995.
24. Obinata G, Anderson BDO. *Model Reduction for Control System Design*. Springer: Berlin, 2001.
25. Hansen FR. A fractional representation approach to closed-loop system identification and experiment design. *Ph.D. Thesis*, Standford University, 1989.
26. Lee WS, Anderson BDO, Mareels IMY, Kosut RL. On some key issues in the windsurfer approach to adaptive robust control. *Automatica* 1995; **31**:1619–1636.
27. Schrama RJP. Accurate identification for control: the necessity of an iterative scheme. *IEEE Transactions on Automatic Control* 1992; **37**:991–994.
28. Ho BL, Kalman RE. Effective construction of linear state-variable models from input–output functions. In *Proceedings of the 3rd Allerton Conference on Communication, Control, and Computing*, University of Illinois, Urbana, IL, 1965; 449–459.
29. Astrom KJ, Bohlin T. Numerical identification of linear dynamic systems from normal operating records. In *Proceedings of the IFAC Symposium on Self-Adaptive Systems*, Teddington, UK, 1965.
30. Zames G. Feedback and optimal sensitivity algorithm: model reference transformations, multiplicative seminorms, and approximative inverse. *IEEE Transactions on Automatic Control* 1981; **26**(2):301–320.
31. Vinnicombe G. Frequency domain uncertainty and the graph topology. *IEEE Transactions on Automatic Control* 1993; **38**:1371–1383.

